Deep Resources Engineering 3 (2026) 100252

Contents lists available at ScienceDirect

Deep Resources Engineering

journal homepage: www.keaipublishing.com/en/journals/deepre/

Full length article

A caprock integrity assessment to optimize CO_2 storage using coupled geomechanics: A case study of the Angostura Field

Adrian Ross *, David Alexander

Energy Systems Engineering Unit, The University of Trinidad and Tobago, Point Lisas, California 540517, Trinidad and Tobago

ARTICLE INFO

Keywords:
Caprock integrity
Sealing performance
Barton-Bandis model
CO_2 trapping mechanism

ABSTRACT

Long-term storage of carbon dioxide (CO_2) in depleted hydrocarbon reservoirs or deep saline aquifers heavily depends on the sealing performance of the caprock. Therefore, it is crucial to evaluate the geomechanical integrity of the caprock since the injected CO_2 can alter the stress regime acting on the rock, potentially leading to rock failure and loss of containment. In this study, we modelled the impact of changes in normal effective stress under a strike-slip stress regime. We tested the sealing performance of the caprock and a sealing shale located approximately 409 m below the caprock under various injection scenarios using the modified Barton-Bandis model. To accomplish this, we constructed a two-dimensional cross-sectional flow model of an offshore depleted gas reservoir and coupled it with the geomechanical module of the CMG-GEM compositional simulator. The primary focus of this research was to conceptually assess the operational and geomechanical parameters, along with the trapping mechanisms that could affect the sealing integrity of the caprock. Simulation results indicated that the caprock would not fail at injection rates below 4531 m^3/d. However, only the lower sections of the sealing shale were fractured under the various injection scenarios. Over a simulation period of 1000 years, the average quantified CO_2 leakage volumes for worst-case flux leakage scenarios were approximately 8137 m^3 (3804,000 kg). Our sensitivity analysis for Young's modulus and Poisson's ratio of the caprock revealed that higher values of Poisson's ratio led to increased lateral expansion. In contrast, a higher Young's modulus resulted in the caprock fracturing more quickly at elevated injection rates. Results also showed that CO_2 injection at lower rates significantly delayed the onset of rock failure. The evaluation of both residual and solubility trapping mechanisms produced similar results. Ultimately, both the caprock and the sealing shale are likely to fail due to shear stress rather than tensile stress. These preliminary results have important implications for evaluating and enhancing CO_2 storage performance.

1. Introduction

Trinidad and Tobago (T&T) plans to reduce its carbon dioxide (CO_2) emissions by 15% in the coming years. As a signatory to the Paris Agreement, T&T has to explore viable options for reducing its carbon footprint. According to a recent carbon inventory, the petrochemical sector accounted for 56% (25.2 million tonnes) of the country's anthropogenic CO_2 [1]. A careful study of the T&T energy sector will reveal the presence of numerous depleted gas fields, largely due to the sector's reliance on natural gas as its primary feedstock. Thus, geological carbon sequestration (GCS) is a technically feasible option for T&T. Although production from mature reservoirs implies that these formations are well characterized. The injection of CO_2 may induce stress changes, which may lead to geomechanical issues such as fault reactivation, ground surface uplift, the propagation of new fractures, and leakage due to caprock failure.

It is the evaluation of the stress changes during the repressurization of the reservoir that forms the basis of a caprock integrity assessment. The assessment is conducted to ensure that the caprock will continue to provide the impermeable seal required to trap the injected CO_2 structurally. Industry experts agree that a caprock should be of sufficient thickness and very low permeability to prevent the migration of hydrocarbons or the injected CO_2 into overlaying areas. While various CO_2 trapping (residual, solubility, and mineral) mechanisms may become active over different geological periods during the sequestration process. The caprock should be considered as the primary trapping mechanism, as it provides a physically impermeable layer that structurally traps the CO_2.

* Corresponding author.
E-mail address: adrian.ross262@utt.edu.tt (A. Ross).

https://doi.org/10.1016/j.deepre.2026.100252
Received 4 April 2025; Received in revised form 19 October 2025; Accepted 5 April 2026
Available online 7 April 2026

Therefore, it is important to conduct caprock integrity assessments to de-risk a potential CO_2 storage site. Many researchers have performed coupled flow geomechanical work to evaluate the stress changes caused by CO_2 injection. Vilarrasa et al. [2] applied a viscoplastic modelling approach to investigate plastic strain trends in an axisymmetric horizontal caprock aquifer system. Their study concluded that the entire caprock may be affected by plastic strain if the horizontal stress is lower than the vertical stress.

Rutqvist and Tsang [3] assessed the sealing integrity of two different caprock scenarios using the TOUGH2-FLAC3D coupled simulator, one with a homogeneous caprock and another intersected by a vertical fault. In both cases, increasing pore pressure resulted in a reduction of effective stress. However, CO_2 leakage occurred only in the faulted caprock system, highlighting the critical role of geological discontinuities in caprock performance. Leakage of CO_2 into the overlaying formation and or back to the surface certainly undermines the primary objective of CO_2 sequestration. This underscores the importance of considering heterogeneous caprock properties and potential failure mechanisms when evaluating storage integrity.

Kim et al. [4] further explored this issue by comparing fracture reactivation in homogeneous versus heterogeneous caprock systems during CO_2 injection into a deep saline aquifer, utilizing the modified Barton Bandis fracture permeability model. Their results demonstrated that heterogeneous caprock systems could store more CO_2 since variations in Young's modulus and Poisson's ratio enabled the caprock to withstand stress changes.

Rutqvist et al. [5] investigated the application of long-reach horizontal injection wells in a thin, low-permeable aquifer. They attributed the observed 5 millimeters per year ground uplift at In Salah to a combination of factors, including increased injection zone pressure, the volume of the injected CO_2, changes in caprock permeability, and the geomechanical properties of the aquifer.

Gillioz et al. [6] conducted a sensitivity analysis to identify key parameters influencing caprock tensile fracturing during CO_2 injection. Using the modified Barton Bandis model, they found that aquifer matrix permeability, Young's modulus of the caprock, and the number of injection wells had the greatest impact on maximizing CO_2 storage while avoiding tensile fracturing.

Alvarez et al. [7] developed an optimization methodology aimed at minimizing caprock failure while maximizing CO_2 storage capacity. Using the CMG-GEM compositional simulator and the CMOST optimization module, they demonstrated that utilizing lower injection rates and pressures over extended time periods would promote greater CO_2 storage through multiple trapping mechanisms while simultaneously reducing geomechanical risks.

All the studies discussed above focused on the geomechanical responses of a caprock subjected to CO_2 injection in a deep saline aquifer. However, few studies focused on using a coupled geomechanical flow model to determine safe operating limits for CO_2 storage in a depleted gas reservoir. Therefore, this study utilized coupled geomechanical numerical simulation to model the effect of stress changes on a caprock and sealing shale for a mature gas reservoir.

The reservoir consists primarily of shelf-edge slope turbidites. Average porosity and permeability for the reservoir were reported as 16% and 285 md, respectively. The reservoir is further characterized by strike-slip tectonics, which have compartmentalized the reservoir. All the wells that penetrated the reservoir encountered the Early Oligocene sand, commonly called the Angostura Sandstone, below a measured depth (MD) of 1387 m. Hydrocarbons are trapped in place by a 106 m thick composite caprock comprising 54 m of Oligo-Miocene Nariva shales and 52 m of Lower Oligocene shale. Another 100 m of the Lower Oligocene Shale sits below the Angostura Sandstone reservoir interval.

The prospective CO_2 storage site (Angostura Field) lies approximately 40 km off the East Coast of Trinidad in Block 2 C. Water depths in the region where the field is located range between 30 to 46 m. Structurally, the reservoir trends northeast to southwest on a hanging wall and forms a 4-way to 3-way faulted anticlinal enclosure. On each flank, the reservoir is bound by a thrust plane that acts as a seal. As pointed out by Narayanan et al. [8], the Angostura sands are made up of two upper slope fan delta turbidite sandstone accumulations. Angostura 1 was drilled into the crest of the 4-way accumulation that trended to the West. Angostura 2 penetrated the 3-way accumulation, which extended to the East, while Angostura 3 was drilled on the southeastern flank. A strike-slip stress regime is present in the reservoir and extends from East to West, producing a strike-slip fault system. This fault system has resulted in substantial lateral movement within the field.

The stress regime of this strike-slip system will be numerically investigated through application of the modified Barton Bandis fracture permeability model. This model is well-defined in the CMG-GEM simulator and serves as a key component of the workflow designed to conceptually assess the integrity of a caprock and sealing shale, helping to de-risk the proposed depleted gas reservoir storage site. Within this workflow, the assessment focuses on understanding how operational parameters, such as injection rate, coupled with geomechanics and CO_2 trapping mechanisms, would affect the sealing performance of the caprock. A two-dimensional (2D) sector of the field was used to demonstrate how much CO_2 can safely be stored in the reservoir without compromising the geomechanical integrity of the caprock.

The 2D model used incorporates petrophysical and geomechanical properties derived from log analysis. The CO_2 injection parameters are investigated using scenarios that model the behavior of the injected CO_2 plume under structural, residual, and solubility trapping to understand its effect on caprock integrity. Data for the mineral composition of the caprock were not available for this study. According to Busch et al. [9], the geochemical interactions between the injected CO_2 and the caprock minerals may strengthen or weaken the sealing integrity of the rock. However, this was not considered for this work. Although the proposed study area is highly faulted, the potential for slip tendency and fault reactivation is not considered in this study. Fig. 1 provides a general indication of the sand quality in the field and highlights the total vertical depth (TVD) at which the caprock and sealing shale are encountered. This present study is intended to serve as a baseline method for performing field-scale assessments aimed at de-risking CO_2 sequestration by evaluating reservoir sealing performance.

This paper is organized into several sections. Section 2 provides an overview of the theoretical framework used in this study, which includes the modified Barton-Bandis model, the Mohr-Coulomb failure criterion, and a discussion of the differences between vertical and horizontal stress. Section 3 outlines the methodology for implementing the Barton-Bandis fracture permeability model to evaluate the sealing performance of the caprock and the sealing shale using a 2D section of the field. In Section 4, the model is validated, and the results from the numerical simulation are analyzed and presented. Finally, the concluding section summarizes the main findings and outlines potential future extensions of this study.

2. Theoretical background

2.1. Modified barton bandis fracture permeability model

As CO_2 is injected into a formation, changes in the total stress (σ) occur as a function of increasing pore fluid pressure (P_f) which is influenced by the Biot coefficient (α) and variations in effective normal stress (σ'_n). The equation linking these parameters together is given below and is known as Terzaghi's law.

$$\sigma = \sigma'_n + \alpha P_f \tag{1}$$

This equation provides the theoretical framework for the operation of the modified Barton Bandis model, which is well defined in the geomechanical module of the CMG simulator. The model is used to simulate geomechanical rock failure as a function of changes in effective normal

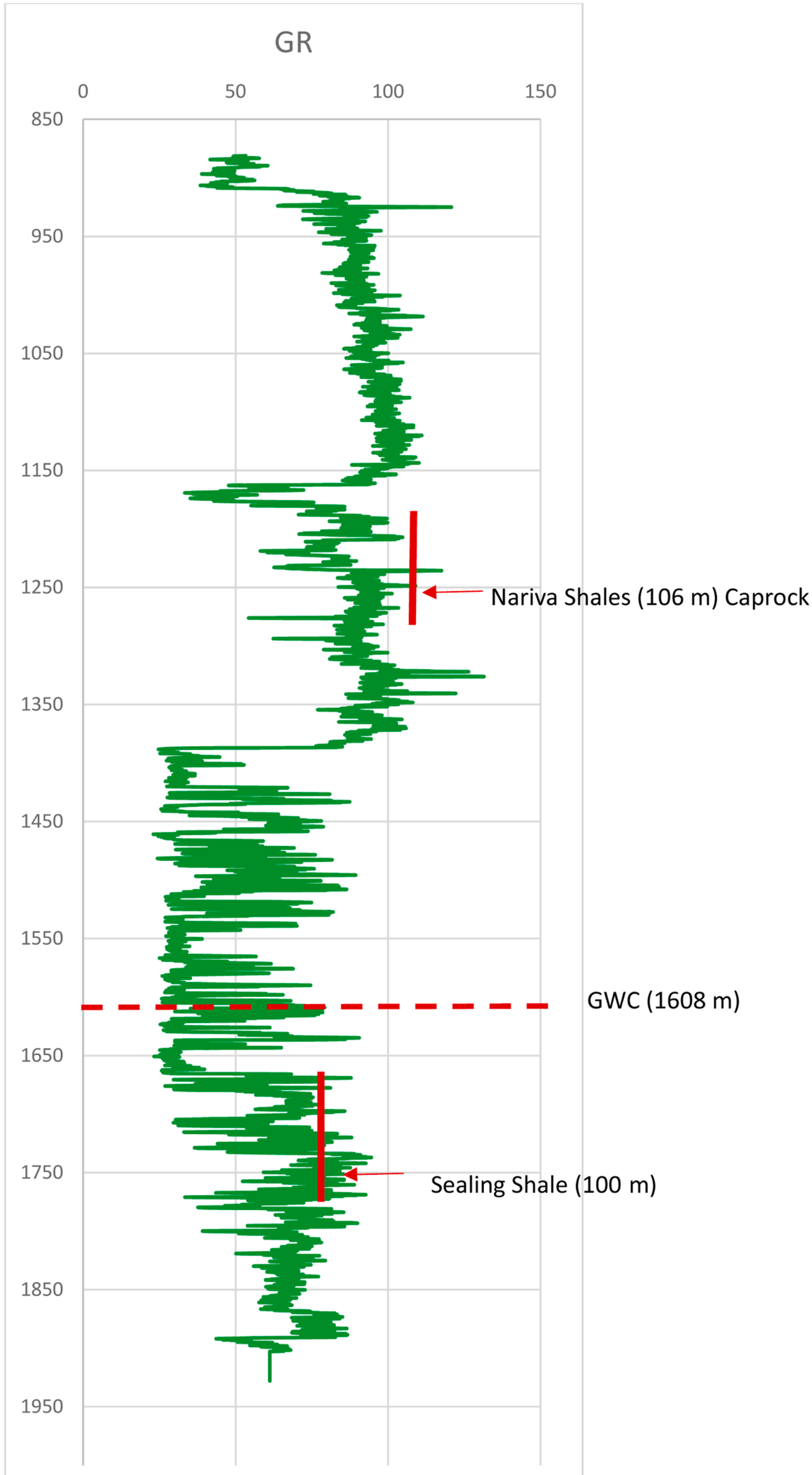

Fig. 1. Gamma ray well log of Angostura 1.

stress during CO_2 injection. In this study, we assume that the sudden increase in fracture permeability (*khf*) is due to the formation of cracks in the rocks.

As illustrated in Fig. 2 (adopted from CMG Ltd, 2022 user guide) [10], if σ'_n is greater than the fracture opening stress (*frs*), permeability will remain along the path AB. This implies that there are no fractures in the rock. However, once σ'_n drops below the *frs* value, the *khf* immediately jumps to its maximum point at C and continues along the path DCE until σ'_n returns to a positive value. At $\sigma'_n > 0$, *khf* falls to the fracture closure permeability (*kccf*) along the path EF. As σ'_n continue to

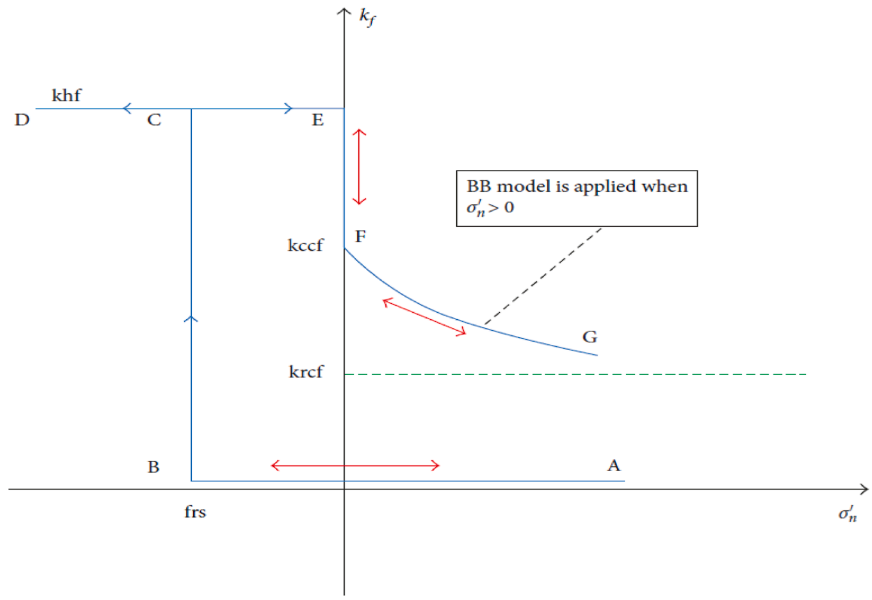

Fig. 2. Barton Bandis fracture permeability model [10].

increase, the fracture permeability moves along a hyperbolic path (FG) to a residual value of fracture closure permeability (*krcf*) since the fracture will not close completely. Paths GFED are reversible, which means that fracture permeability is affected by its history.

Unlike the Mohr-Coulomb (M-C) failure criterion discussed in Section 2.3, the Barton Bandis model is non-linear. While both models are utilized for analyzing the shear strength of a rock, the Barton Bandis model considers the joint compressive strength and roughness to model joints and fractures. In contrast, the M-C model is linear and computes shear strength based on cohesion and internal angle of friction [11].

2.2. Vertical horizontal stress and Biot's constant

The effective stress (σ'_n) described in Eq. (1) acts only in the vertical direction and thus represents the vertical effective stress. Eq. (2) shows the derivation of the relationship as the overburden or total stress (σ) minus the pore pressure.

$$\sigma'_n = \sigma - \alpha P_f \tag{2}$$

Where α is the Biot coefficient, which governs how pore pressure impacts effective stress and is given below as cited in literature [12]. Ø is the average porosity.

$$\alpha = 0.64 + 0.854(\varnothing) \tag{3}$$

It is important to make this distinction since horizontal stress controls the activation of the fracture in the Barton Bandis model. The minimum horizontal stress (σ_h) was estimated using Eq. (4) [12].

$$\sigma_h = \frac{\nu}{1-\nu}.(\sigma - \alpha P_f) + \alpha P_f + P_{tec} \tag{4}$$

P_{tec} – represents the pressure due to tectonic activity and is assumed to be 5000 kPa; ν – the value for Poisson's ratio.

2.3. Mohr- Coulomb failure criterion

The Mohr-Coulomb (M-C) is given by Eq. (5). As cited in Labuz and Zang [13], this equation was introduced by Coulomb, who stated that the shear strength can be expressed as a linear function of cohesion and normal stress. However, Mohr found that failure depended on the maximum principal stress (σ_1) and the minimum principal stress (σ_3).

$$\tau = c + \sigma_n \tan\varphi \tag{5}$$

Where τ – is the value of shear stress at the point of failure; c – is the value for cohesion, which defines material internal shear strength; σ_n – is the normal stress acting on the plane; φ – angle of internal friction, which defines the material's resistance to shear stress.

According to Jiang and Xie [14], M-C is generally applied when compressive stresses are at work. However, the M-C model can be modified (see Eq. (6)) to account for positive tensile stress since under this stress state, the material is pulled apart, which can affect the failure criterion. Thus, failure would be due to tensional forces as opposed to shear forces. The M-C equation remains the same except for the sign change to negative. This change in sign indicates that an increase in tensile stress would reduce the material's susceptibility to shear failure.

$$\tau = c - \sigma_n \tan\varphi \tag{6}$$

Where σ_n – is the tensile stress acting on the plane.

In this study, both forms of the equations were used to validate the simulator results for fracture activation by determining the tensile/shear stress of the sealing shale and the caprock.

3. Methods

3.1. Model description

To assess the sealing integrity of both rocks, several simulations were conducted using a 2D cross-sectional model. The CMG-WINPROP PVT simulator was used to tune a fluid model based on lab data for the field. One producer well was placed in the model and choked at 339,802 m^3/d to replicate the recovery factor of the field for a production period of 9 years. Cartesian grids were used to construct the model, which consisted of 34 blocks in the horizontal direction and 22 blocks in the vertical direction. The model extended laterally to 2865 m and 636 m vertically, with a width of 30.5 m.

Fig. 3 shows the model, which consists of one 106 m caprock layer and one 100 m sealing shale layer located approximately 409 m below the caprock. For both the caprock and the sealing shale, the permeability is set to 1.0×10^{-8} md to depict a no-flow boundary. The model was initialized in CMG- GEM with a dual permeability grid to implement the modified Barton Bandis fracture permeability model. To reduce

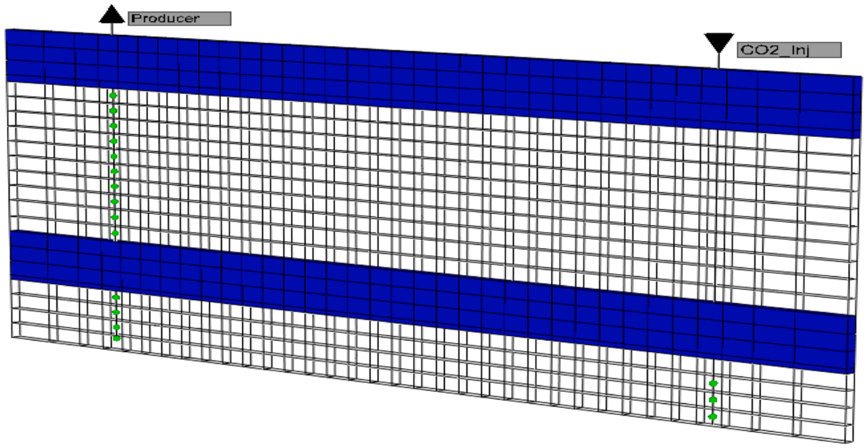

Fig. 3. 2D Cross-section reservoir model of the Angostura Field.

computational time and to increase the resolution in proximity to the wells, grid sizes were increased in increments of 76 m up to 152 m towards the outer boundaries of the model. An overview of the workflow used in this study is given in Fig. 4.

A summary of the reservoir properties is shown in Table 1. The production well is perforated above and below the sealing shale. However, for the injection well, the perforations are set only below the sealing shale for the purpose of inducing a fracture, which would cause the CO_2 to move into the layers above until it encounters the caprock. Initially, only structural trapping was modelled since this mechanism would take effect from the beginning of CO_2 injection. Other mechanisms are evaluated later to test their effect on the caprock integrity.

The mole percentages for the respective components used in the fluid model are given in Table 2.

Table 1
Reservoir parameters of the Angostura Field.

Reservoir properties parameters	Value
Area of 2D sector (km^2)	1
Initial pressure (MPa)	19
Reservoir temperature (°C)	89
Average porosity (%)	16
Average permeability (mD)	285
Rock compressibility (Pa^{-1})	3.40×10^{-9}
Reservoir interval (m)	1268–1607
Gas water contact (m)	1608

3.2. *Estimation of geomechanical properties*

Three rock types were used in the model, as displayed in Table 3. To evaluate the geomechanical integrity of the caprock and the sealing shale, rock types 1 and 3 were defined using the Mohr-Coulomb failure criterion. In contrast, rock type 2 was defined using the Drucker-Prager model. For all cases modelled, the value for cohesion, which affects the yield state of the rock, was set to 689,476 kPa. Therefore, the model was assumed to be fully elastic.

The mechanical properties of these rocks were estimated using log-based correlations with Eqs. (7–14). The main inputs were the velocities from shear and compressional waves.

$$E_{\mathrm{dyn}} = \frac{\rho V_s^2 (3V_p^2 - 4V_s^2)}{(V_p^2 - 2V_s^2)} \tag{7}$$

$$\nu = \frac{V_p^2 - 2V_s^2}{2(V_p^2 - V_s^2)} \tag{8}$$

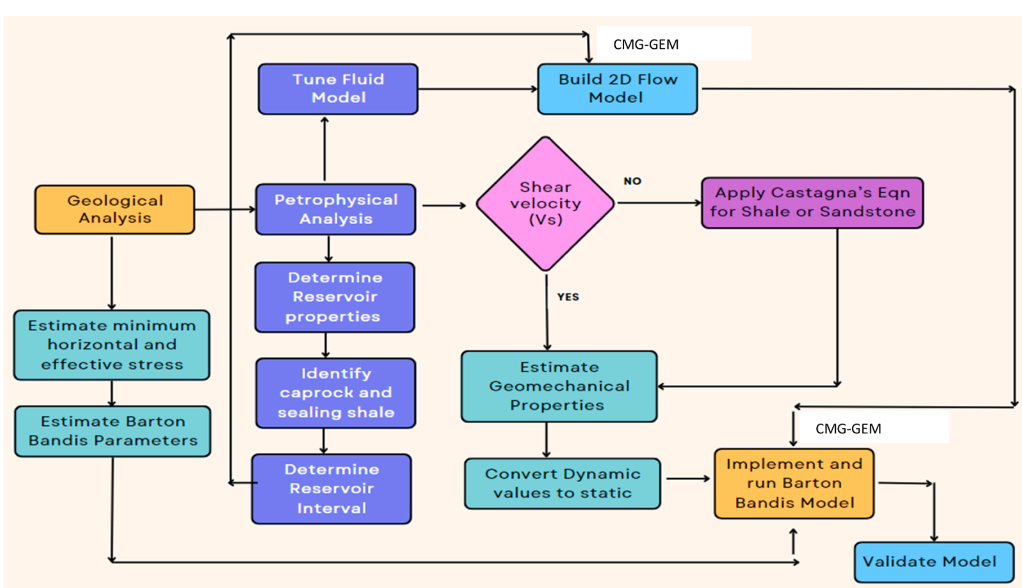

Fig. 4. Overview of study workflow.

Table 2
Reservoir fluid composition for Angostura.

Component	Mole fraction (%)
CO_2	0.991
N_2	0.797
C1	94.259
C2	2.773
C3	0.530
IC4	0.189
NC4	0.202
IC5	0.099
NC5	0.069
C6	0.065
C7+	0.026

Table 3
Geomechanical properties of the Angostura Field used in the 2D base model.

Rock type	Young's modulus (GPa)	Poisson's ratio	Rock compressibility (Pa^{-1})
Caprock (1)	1.51	0.22	3.40×10^{-8}
Sand layers (2)	22.59	0.19	3.40×10^{-9}
Sealing shale (3)	3.46	0.20	3.40×10^{-9}

$$V_s = 0.769V_p - 0.867 \text{ Castanga's model for shale} \tag{9}$$

$$V_s = 0.804V_p - 0.856 \text{ Castanga's model for sandstone} \tag{10}$$

$$E_{\text{sta}} = 0.0491E_{\text{dyn}} + 0.7079 \text{ Wang's model for shale} \tag{11}$$

$$E_{\text{sta}} = 0.4145E_{\text{dyn}} - 1.0593 \text{ Wang's model for sandstone} \tag{12}$$

$$K_{\text{n}} = \frac{\sigma'_n}{b} \tag{13}$$

$$K_{\text{f}} = \frac{b^2}{12} \tag{14}$$

Where E_{dyn} is the dynamic Young's modulus, while v is Poisson's ratio [15]; V_s – is the value of the shear wave velocity (m/s) given by Castagna et al. [16] when V_s is not available; E_{sta} – is the static Young's modulus given by Wang's model for shale and sandstone, which provides an estimate based on laboratory studies [17]; V_p – is the value of the compressional wave velocity (m/s); ρ – is the bulk density of the rock in (kg/m^3); K_{n} – is the Godman normal fracture stiffness [18], where b is the change in the fracture aperture in ft; K_{f} – is Barton Bandis fracture permeability, calculated using the cubic law, which does not account for stress changes [19].

The parameters used to enable the Barton Bandis model are given in Table 4. Analysis of data taken from core samples and outcrop by Gale et al. [20] showed that the fracture aperture of many shales falls in the range 3.048×10^{-5} to 1.016×10^{-3} m. The higher range was used in the base model.

Estimated value for vertical effective (z or σ'_n) stress used in the model was 23.67 MPa. The value for horizontal stress, which represents the stress acting in the I and J directions, was estimated at 22.27 MPa.

Table 4
Parameters used to implement the Barton Bandis Model in the Base Case.

Parameters	Value
Eo, Initial fracture aperture (m)	1.016×10^{-3}
Kni, Initial normal fracture stiffness (Pa/m)	8.076×10^{9}
frs, Fracture opening stress (kPa)	22,270
khf, Hydraulic fracture permeability (md)	920×10^{6}
kccf, Fracture closure permeability (md)	920×10^{6}
krcf, Residual fracture closure permeability (md)	920×10^{6}

3.3. Derivation of injection rate

To obtain a range of practical injection rates, a review of actual carbon capture field projects was conducted. As was pointed out by Ghaderi et al. [21], the general rule of thumb is to use an injection rate of 1 Mt/year to evaluate CO_2 storage performance. Table 5 shows that the annual injection rate for the In Salah and Sleipner projects is closer to the recommended value than that of the K12-B project. A comparison of Angostura parameters indicates that the properties listed are more closely related to those found in K12-B projects. Therefore, the base model should use an injection rate of 56,634 m^3/d or 53 t/d, as the field modelled in this study is more than twice the size of the K12-B in terms of acreage. However, since the 2D represents 2% of the full field, one injector with an injection rate of 1133 m^3/d was used as the base rate. With the base case set up, a series of sensitivity analyses was performed to investigate the impact of various parameters on the caprock integrity.

3.4. Residual trapping

Residual trapping mechanism traps the injected CO_2 due to hysteresis in the relative permeability. As the injected CO_2 moves through the pore space in the rock, the saturation of CO_2 shifts from drainage (CO_2 displacing resident reservoir fluid) to imbibition (the reservoir fluid flows back into the pore space) and immobilizes the CO_2. To simulate this trapping mechanism, the Land hysteresis model was applied. To estimate the maximum residual gas saturation (S_{grm}), which is a required input for the Land hysteresis model, Eq. (15), known as Holt's equation, was applied. Using the average value for porosity ($\varnothing$) (See Table 1), the estimated S_{grm} was found to be 0.39.

$$S_{\text{grm}} = -0.9696\varnothing + 0.5473 \tag{15}$$

3.5. Solubility trapping

To model solubility trapping, Li-Nghiem's method for Henry's law constant was applied as a correction to the Peng-Robinson equation of state (PR-EOS) for predicting solubility. This correlation estimates the fraction of injected CO_2 that dissolves in the formation water under reservoir conditions. Henry's coefficient, which relates the CO_2 partial pressure in the gas phase to its mole fraction in the aqueous phase, was calculated at reservoir temperature and pressure (Table 1). Additionally,

Table 5
Comparison of the characteristics of the three CCS projects with Angostura.

Parameter	In Salah	Sleipner	K12-B	Angostura
Annual reported injection rate (Mt/year)	0.74 [22]	0.8 [26]	0.2 [23]	-
Years active	7 [23]	24 [26]	~15 [29]	-
Reservoir area (acres)	494,211 [24]	6424,740 [28]	6178 [a]	12,788
Volume stored (million Mt)	3.8 [23]	18.5 [26]	> 0.1 [30]	-
Average injection rate per day (t)	1487 [a]	2667 [a]	53 [a]	-
Aquifer thickness (m)	66 [25]	656 [26]	-	-
Porosity (%)	11–20 [25]	35–40 [27]	8–12 [30]	16
Permeability (mD)	10 [25]	1000–8000 [27]	5–500 [29]	285

Note: This table was compiled using sources listed hereunder. Oldenburg et al. [22], Carbon Capture and Sequestration Technologies MIT [23], Ringrose et al. [24], Mathieson et al. [25], [a] Values estimated based on reported figures, Williams and Chadwick [26], Baklid and Korbol [27], Torp and Gale [28], Vandewwijer et al. [29], Vandewwijer et al. [30], Audigane et al. [31].

binary interaction parameters in the PR-EOS were tuned to ensure realistic solubility behavior.

4. Results and discussion

4.1. Analytical model validation

The simulation results for fracture pressure were validated using both derivations of the M-C as outlined in Section 2.3. Assumed values for cohesion and internal friction angle were 5006 kPa and 30°, respectively. This postulation was based on analogous data from a laboratory report on sandstone rock strength. It was assumed that the cohesion value for shale would be 50% lower according to the mineral and grain composition of the shale [32]. Using the reported overburden gradient (20.36 kPa/m), the normal stress values were computed as 23,670 and 32,095 kPa for the caprock and sealing shale, respectively. It was found that the failure mode is primarily influenced by the dominant horizontal stresses present in the reservoir, leading to shear failure (Table 6).

A difference of approximately 3% between the M-C shear stress analytical solution and the simulator results for the caprock indicates that the rocks are more prone to shear failure than tensile failure. While the difference between the M-C shear stress and the simulator for the sealing shale was approximated as 24%. This suggests that the assumed values for cohesion and internal friction angle may be vastly different for the sealing shale. As was pointed out by Chang et al. [32], rocks exhibit more weakness in tension and thus fail at a lower tensile stress compared to the higher values required for shear failure. This explains the large difference between the results for tensile failure versus shear failure obtained using the M-C tensile and shear failure models.

4.2. Effect of injection rate on fracture propagation

To study the effect of injection rate on the fracture propagation of both rocks, the injection rates were varied in increments of 1133 m^3/d up to 5663 m^3/d. Only the fracture domains for the sealing shale and the caprock were considered. Injection was set to begin in February 2025. CO_2 was injected until the sealing shale fractures. When the sealing shale fractures, it was expected that the injected CO_2 would leak into the upper layer until it encounters the caprock. However, due to the thickness (100 m) of the sealing shale, the fracture only propagated 70 m into the rock. This meant that no CO_2 leaked into the layers above the sealing shale.

Fracture propagation refers to the growth and lengthening of fractures within a rock unit as it undergoes variations in stress. In this study, it is assumed that a change in fracture permeability as defined in the Barton Bandis model is synonymous with the formation and propagation of fractures. Observations of the sealing shale indicate that the fracture extended vertically by 70 m, as depicted by the increase in fracture permeability, which is highlighted by red grid blocks shown in Fig. 5. Notably, for all injection rates under this scenario, the length of the fracture remained constant while the fracture propagated vertically. This indicates that the upper layers of the sealing shale were unaffected, as the increase in pore pressure and the corresponding reduction in normal fracture effective stress (N_{fres}) were minimal. Similar findings were reported by Rutqvist and Tsang [3].

Table 6
Comparison between simulator and analytical solutions.

	Analytical solution caprock	Analytical solution sealing shale
M-C for shear stress (kPa)	18,671	23,547
M-C for tensile stress (kPa)	8660	13,521
	Caprock	Sealing shale
Simulator solution (kPa)	19,271	17,961

For the caprock scenario, the CO_2 injection well was perforated 213 m below the caprock, as shown by the yellow circles in Fig. 6. The results indicate that the fracture extends into the upper layers of the sealing shale because the injection occurs close to this rock layer. Similar to the case for the sealing shale, there was no change in the fracture propagation for varying injection rates up to 5663 m^3/d. Fig. 6 provides an overview of how the fracture affects the top of the sealing shale and the bottom of the caprock. Only 14 m of the caprock was fractured compared to 100 m of the sealing shale being fractured under this scenario. Therefore, no leakage to the surface was observed.

In the caprock scenario, the injection rate was further increased to determine the threshold at which the entire rock would fracture. It was found that the entire caprock would fracture at an injection rate of 6796 m^3/d, which corresponded to an injection pressure of 19.27 MPa. The propagation of the fractures affects the top section of the sealing shale, while the entire caprock was fractured as indicated by the change in permeability in Fig. 7.

An observation well was integrated into the model to estimate the CO_2 worst-case flux leakage scenario. After the entire caprock failed in the year 2684, the injector well was shut in, and the volume of leaked CO_2 was recorded, as shown in Fig. 8. It was noted that 8137 m^3 of CO_2 had leaked from the reservoir. Prior to the failure of the entire caprock, a total of 1.61 billion cubic meters (bcm) of CO_2 had been injected. Consequently, this represents only 5.05×10^{-6}% of the injected CO_2 that leaked.

4.3. Effect of injection rate on time of fracture

The CO_2 injection well was perforated above the sealing shale to test the sealing performance of the caprock. The date for each of the rocks to fracture at the various injection rates is summarized in Table 7, recorded as YY-MM-DD. The models were simulated for 1000 years, and the cumulative volume of CO_2 injected at the time of caprock failure was recorded. It was assumed that the volume of CO_2 injected is equal to the volume of CO_2 stored by structural trapping.

These results indicate that it may be best to inject at a lower rate for a longer time since 314 million m^3 was stored using the injection rate of 1133 m^3/d without caprock failure. However, some studies suggest that this option may prove to be uneconomical on a field scale [6]. In addition, for the cases with an injection rate below 4531 m^3/d, the pressure does not increase substantially to cause the caprock to fracture. For the highest injection rate of 5663 m^3/d, the time taken for both rocks to fracture is significantly reduced compared to the other cases. This is because at the higher injection rate, the reservoir pressure is expected to build up much faster, leading to earlier fracturing of the rocks.

Further analysis of the results confirmed the previous findings of Gonzales Martinez de Miguel [33], which showed that the relationship between time taken for fracture and cumulative injected volume of CO_2 is exponential rather than linear, as illustrated in Fig. 9. These results confirm that a reduction of the injection rate could improve CO_2 storage capacity, as the caprock will not fracture using the base case injection rate. Additional sensitivities on injection rate indicate that the caprock would first fracture at an injection rate of 4531 m^3/d. The simulation results indicate that below this threshold, the caprock would not fracture. Once the caprock fractures, the permeability jumps to the pre-set value as shown in Fig. 10. A similar plot is provided for the sealing shale as depicted in Fig. 11.

4.4. Effect of injection rate on fracture pressure

It was observed that the fracture pressure was small relative (see Table 8) to the depth, as the in-situ stress regime has a direct effect on the magnitude of fracture pressure [34,35]. This result can also be attributed to the increase in pore pressure as described in Terzaghi's law.

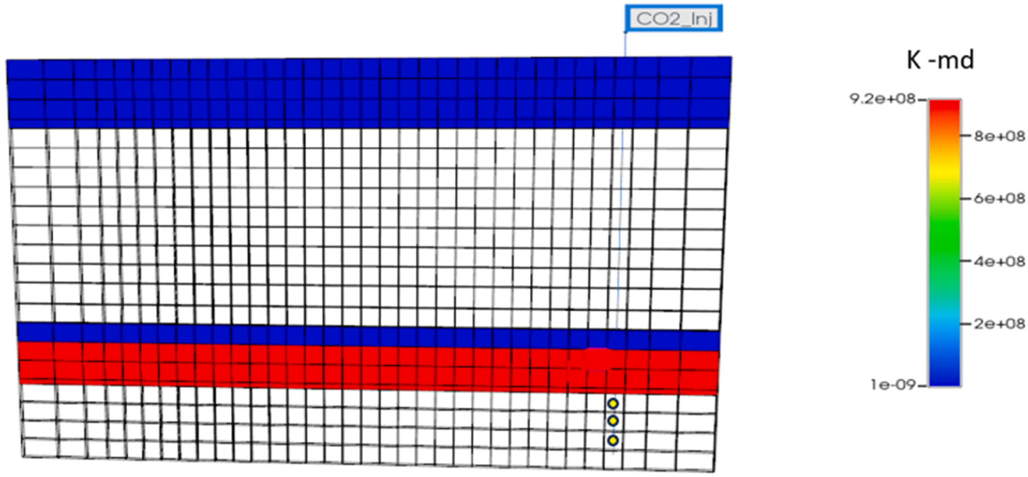

Fig. 5. Vertical fracture propagation observed for CO_2 injection below the sealing shale.

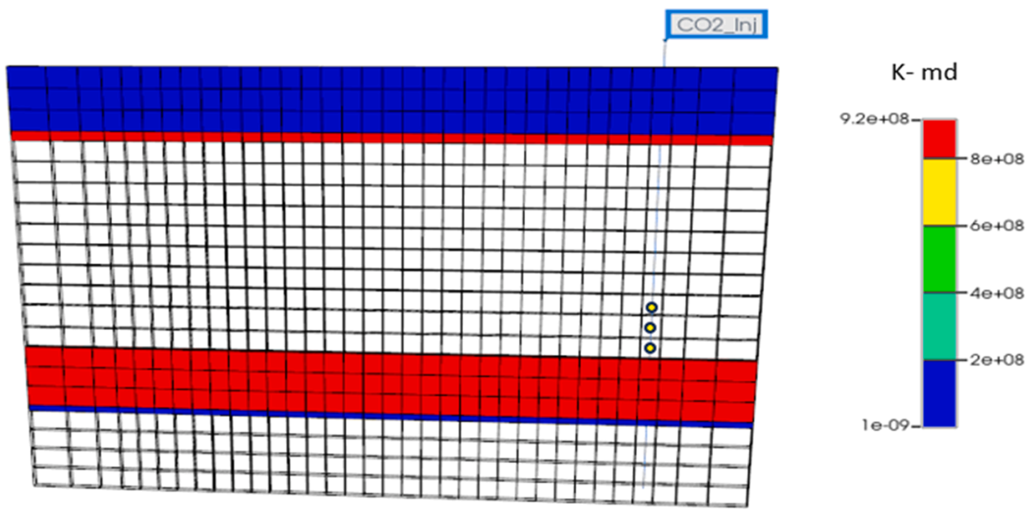

Fig. 6. Vertical fracture propagation observed for CO_2 injection below the caprock.

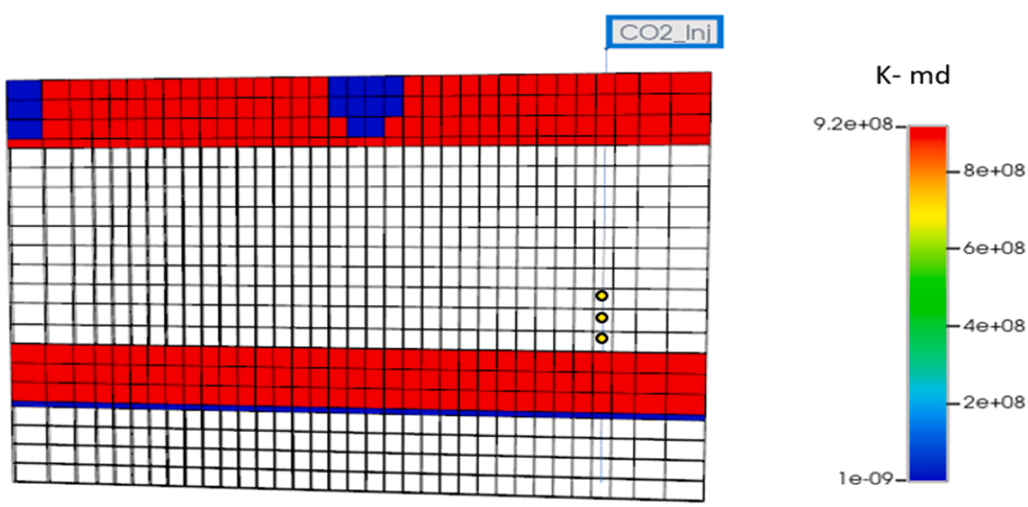

Fig. 7. Vertical fracture propagation observed for the entire caprock.

The σ_h represents the least principal stress for a strike-slip stress regime according to Anderson's classification $\sigma_H > \sigma_v > \sigma_h$. Injection of CO_2 induces a decrease in the $N_{\text{fres,}}$ which causes the fracture to propagate in a vertical direction perpendicular to the least principal stress, requiring a small change in vertical fracture pressure, as illustrated in Fig. 12.

Comparison of the fracture pressures for both rocks showed that repressurization of the reservoir close to the initial reservoir pressure causes the fractures of the sealing shale. In contrast, incremental

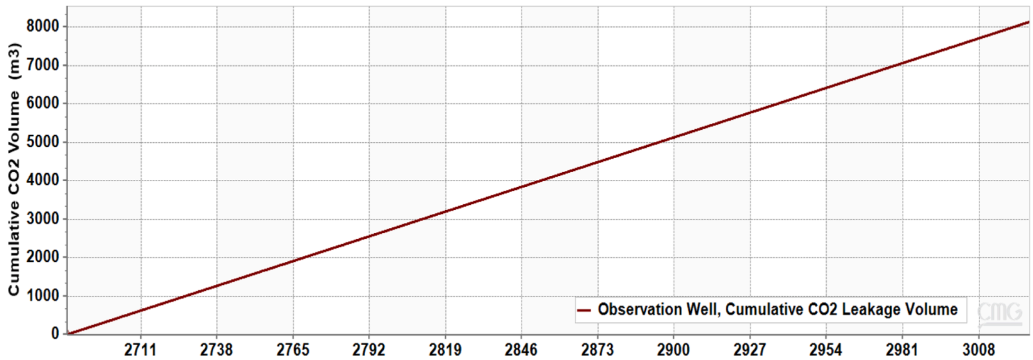

Fig. 8. Cumulative volume of CO_2 worst case flux leakage after caprock failure.

Table 7
Summary of effect of injection rate on fracture opening time.

Injection rate (m^3/d)	Sealing shale fracture (Date)	Caprock fracture (Date)	Time difference between fracture of both rocks (Years)	Volume of CO_2 injected at caprock fracture (bcm)
1133	2152/09/12	-	-	-
2265	2088/09/12	-	-	-
3398	2067/09/12	-	-	-
4531	2057/09/12	3008/09/12	951	1.61
5663	2051/09/12	2824/09/12	773	1.64

increases above the initial reservoir pressure results in the fracture of the caprock.

4.5. *Effect of geomechanical parameters on fracture opening time*

To test the effect of the two main geomechanical parameters, sensitivities were performed using the values shown in Table 9. Each of the simulated scenarios was compared against the base case. When the values for Young's modulus were varied, the values for Poisson's ratio remained set at the base case value. The opposite was done for sensitivity analysis using Poisson's ratio.

4.5.1. *Young's modulus*

Generally, when compared to sandstone, shales exhibit lower geomechanical values for Young's modulus and higher values for Poisson's ratio [32,36]. The difference can be attributed to the finer grains found in shales and their overall mineral composition. Therefore, in this study, it is assumed that the Young's modulus for Shale is 50% higher than the estimated the base case values which were initially low. A similar assumption was made for the value of Poisson's.

As illustrated in Fig. 13, the caprock rock experienced negligible changes in vertical displacement compared to the base case. This can be attributed to a lower Young's modulus, which makes the rock more ductile, meaning it bends more when subjected to CO_2 injection. Therefore, a minor increase in deformation is observed for the base case before the fracture of the caprock.

Fig. 14 depicts the changes in porosity (Geo-corrected) due to geomechanical effects such as compaction and changes in stress. The vertical red arrow on the figure indicates that during the reservoir depletion phase, porosity decreases from its initial value. This shows that the pores are closing as a result of a decrease in pore pressure. However, as the pore pressure begins to increase due to CO_2 injection, the pores begin to re-open, resulting in the observed reverting of porosity to in-situ values.

A delay in fracture time of 3 years for the caprock at an injection rate of 5663 m^3/d was observed for the higher value of Young's modulus, as shown in Fig. 15. While the caprock was fractured at an injection rate of 4531 m^3/d for the base case, no fracture was observed at this same rate using the higher value for Young's modulus.

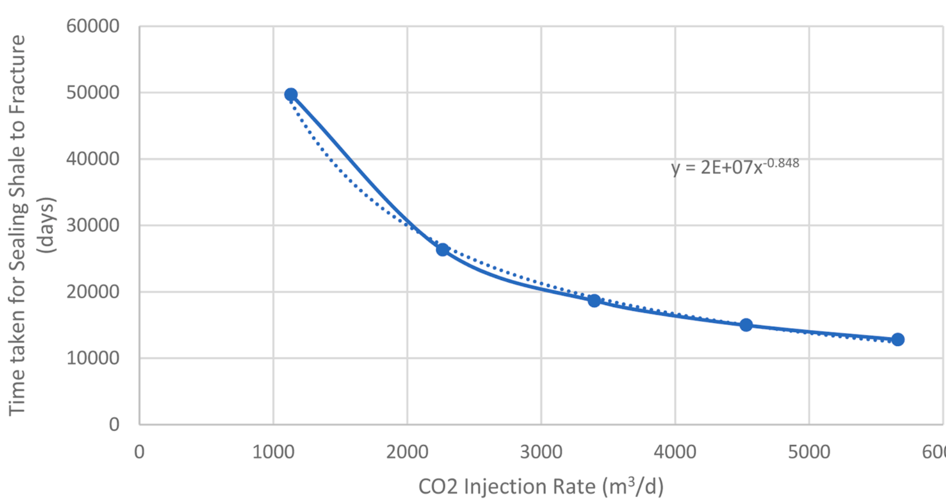

Fig. 9. Plot of injection rate vs time taken for sealing shale failure.

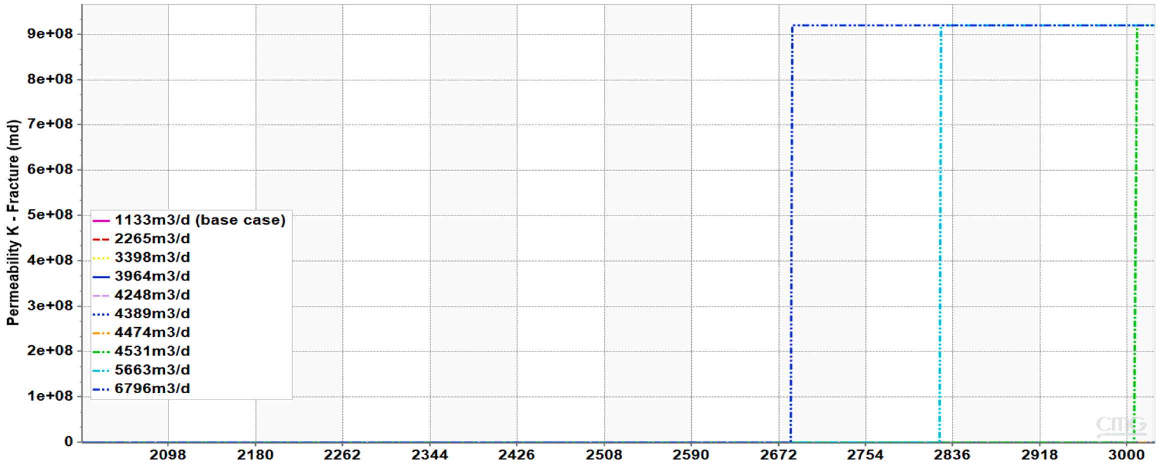

Fig. 10. Effect of injection rate on time taken for fracture of the caprock.

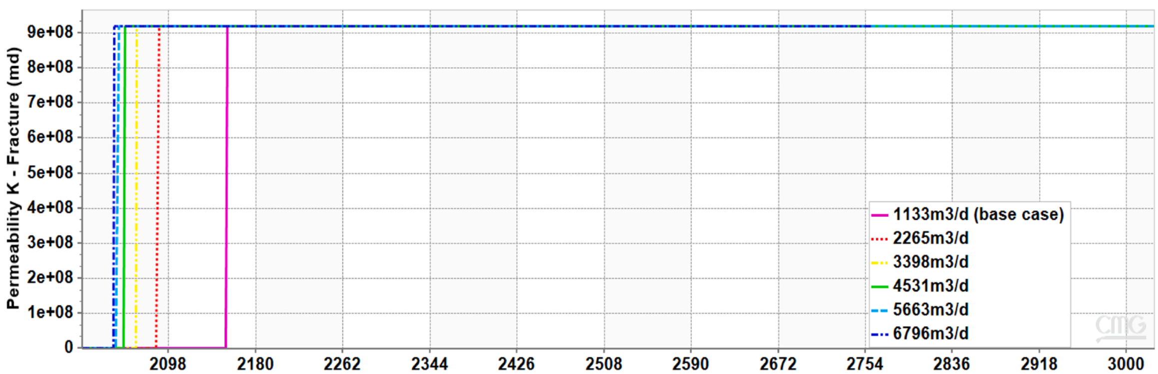

Fig. 11. Effect of injection rate on time taken for fracture of the sealing shale.

Table 8
Comparison of fracture pressure and injection rate.

Injection rate (m^3/d)	Fracture pressure of sealing shale (kPa)	Fracture pressure of caprock (kPa)
1133	18,044	-
2265	18,409	-
3398	18,064	-
4531	17,547	19,223
5663	17,754	19,236
6796	18,443	19,271

Table 9
Geomechanical parameters used in sensitivity analysis.

Parameter	Sealing shale	Caprock
Young's modulus (GPa) sensitivity case	6.92	3.01
Young's modulus (GPa) base case	3.45	1.51
Poisson's ratio sensitivity case	0.30	0.33
Poisson's ratio base case	0.20	0.22

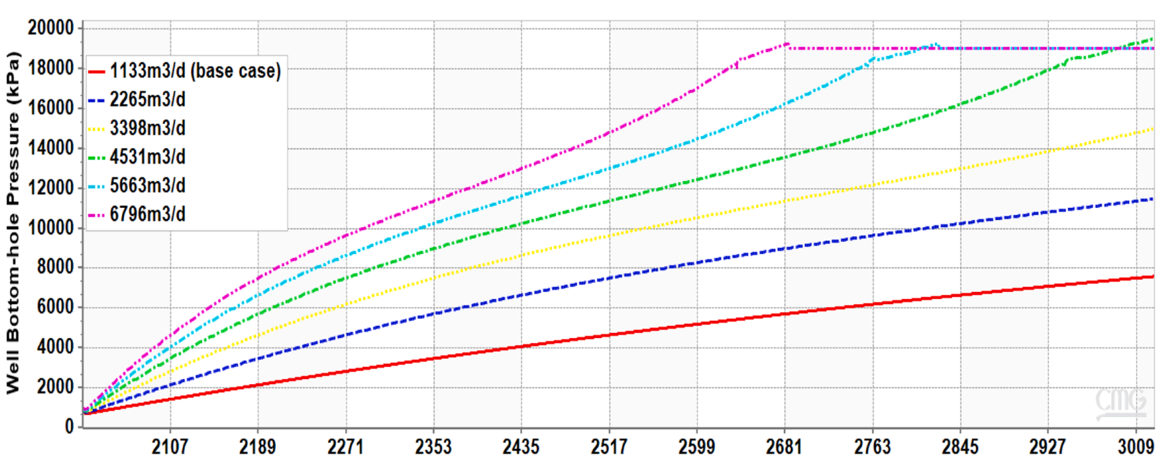

Fig. 12. Effect of injection rate on fracture pressure.

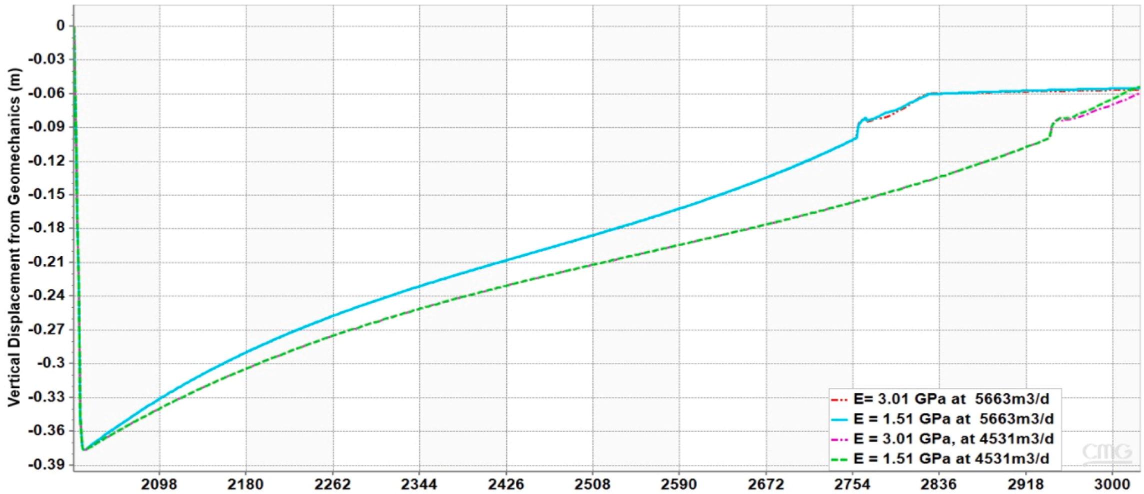

Fig. 13. Comparison of vertical displacement for sensitives on Young's modulus.

4.5.2. Poisson's ratio

Poisson's ratio controls the lateral expansion of the rock when stress or pressure is applied vertically. Therefore, the analysis of the results focused on determining if there were changes in lateral expansion. The results showed that more lateral displacement occurred when a higher value was used in the model, as shown in Fig. 16.

Although the caprock experiences a greater amount of lateral expansion at the higher value for Poisson's ratio, this had no effect on the time of fracture of the rock at an injection rate of 5663 m^3/d, as illustrated in Fig. 17. However, at the injection rate of 4531 m^3/d, when the value for Poisson's ratio was higher, the caprock fracture time was delayed by 14 years. Thus, a lower injection rate with a higher Poisson ratio resulted in slower pressure build-up and better strain distribution.

4.6. Effect of trapping mechanisms on caprock integrity

The base case only considers structural trapping. In this section, residual and solubility, and trapping were modeled to study the effect of each of these mechanisms on caprock sealing integrity and failure time. From the base model, it was found that the caprock first fracture was observed at an injection rate of 4531 m^3/d. Thus, the base case model with injection rates of 4531 to 6796 m^3/d was utilized to model the scenarios for residual and solubility trapping. At the lower injection rate, 1.66 bcm of CO_2 was stored without caprock failure. However, at the higher injection rates, more CO_2 was stored compared to the base case.

The results for modeling of residual and solubility showed that these trapping mechanisms will slow the migration of CO_2 and, in turn, delay caprock failure. Under this scenario, it was observed that the caprock would first fracture at an injection rate of 6796 m^3/d. Summing the amount of CO_2 stored for a particular injection rate would give the total amount of CO_2 stored at that rate, as shown in Table 10.

On average, at least 24% of the injected CO_2 is stored by solubility trapping, while residual accounts for an average of 23%. Although these mechanisms have been modelled, the greater amount of CO_2 remains in the free state in the reservoir and is trapped structurally. Structural tapping accounted for an average of 52% of the injected CO_2.

Table 11 shows the comparison of the fracture date for the base case, which only considered structural trapping versus the trapping mechanisms for residual and solubility. The results indicate that there is a significant increase (time delay) in the time taken for the caprock to fracture when residual and solubility trapping are considered. It was found that the injection rate between 4531 and 5663 m^3/d, the caprock

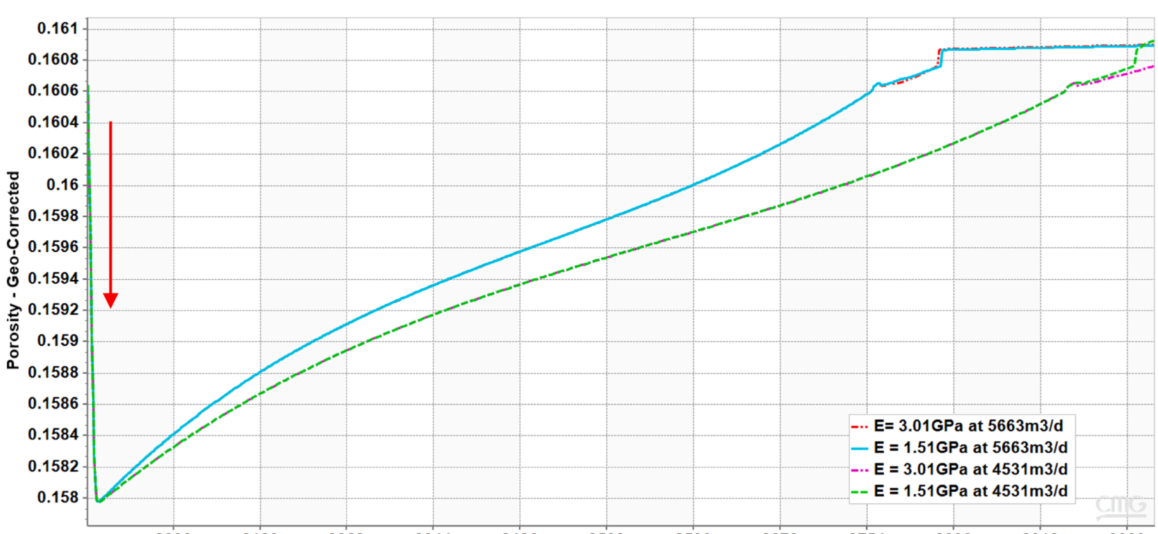

Fig. 14. Comparison of geo-corrected porosity for sensitives on Young's modulus.

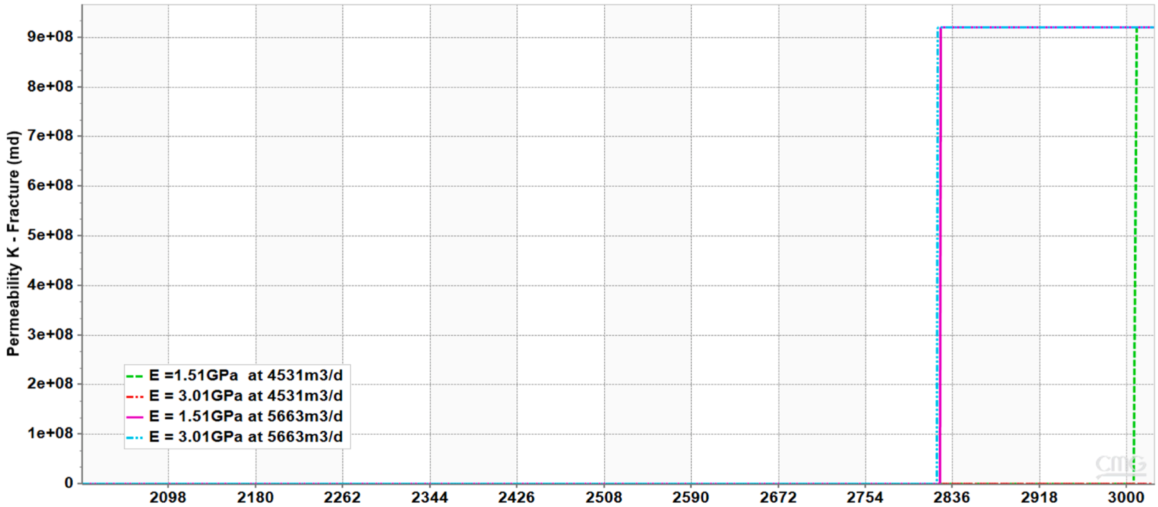

Fig. 15. Comparison of fracture time for sensitives on Young's modulus.

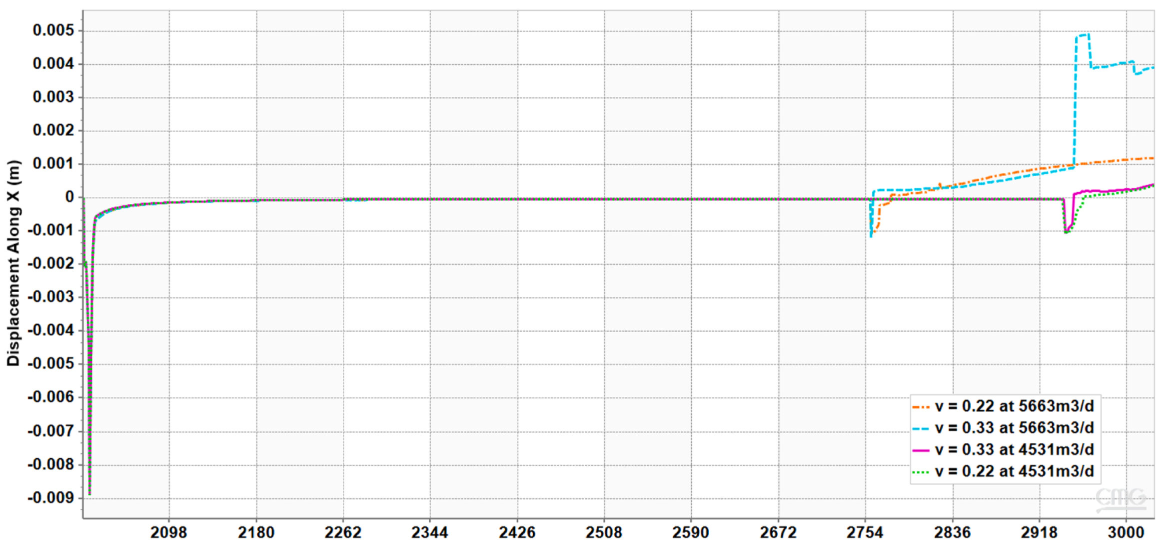

Fig. 16. Comparison of displacement along the X for sensitives on Poisson's ratio.

Fig. 17. Comparison of fracture time for sensitives on Poisson's ratio.

Table 10
Volume of CO_2 trapped by the different mechanisms.

Injection rate (m^3/d)	Date of caprock failure	Total CO_2 structurally (bcm)	Total CO_2 residual (bcm)	Total CO_2 solubility (bcm)
4531	-	0.88	0.41	0.36
5663	-	1.10	0.46	0.55
6796	2856/09/12	1.32	0.61	0.61

Table 11
Comparison of caprock fracture time for base case vs trapping mechanisms.

Injection rate (m^3/d)	Date of caprock failure for base case	Date of caprock failure with trapping mechanisms	Trapping mechanisms time difference in caprock failure (years)
4531	3008/09/12	-	-
5663	2824/09/12	-	-
6796	2684/09/12	2856/09/12	172

would not fracture when residual and solubility trapping is considered. This result can be attributed to the reduction of the movable CO_2 in the reservoir.

As such, the caprock would be exposed to a reduced buoyancy force of CO_2. Therefore, the injection rate was incrementally increased until a fracture was observed at a rate of 6796 m^3/d. However, it was observed that the fracture did not propagate through the entire caprock. Therefore, there was no leakage of CO_2 to overburden layers.

5. Conclusions

This study evaluated caprock integrity for a depleted offshore gas reservoir using the modified Barton–Bandis fracture permeability model within CMG-GEM. The results indicate that both the caprock and sealing shale are more susceptible to shear failure than tensile failure due to the strike-slip stress regime, which is dominated by horizontal stresses. Key findings include:

- Injection rate control is critical for maintaining caprock integrity. CO_2 can be safely stored at approximately 314 million m^3 when injected at 1133 m^3/d, while vertical fracture initiation occurs only at rates above 4531 m^3/d (fracture pressure ~19.2 MPa).
- The occurrence of fractures in the sealing shale at lower injection rates is explained by the elevated Young's modulus, which resulted in increased brittleness.
- A non-linear relationship was observed between injection rate, fracture opening, and fracture propagation.
- Sensitivity analysis showed that a higher Poisson's ratio increased lateral expansion, while a higher Young's modulus led to faster fracturing at elevated injection rates.
- Residual and solubility trapping mechanisms were found to reduce leakage risk by slowing upward CO_2 migration.
- Differences between model predictions and Mohr-Coulomb estimates emphasize the need for laboratory testing of cohesion and friction angle to improve model accuracy.

Overall, the study demonstrates that fracture pressure is highly dependent on the stress regime. Under strike-slip conditions, fractures in the sealing shale could initiate at pressures as low as 17.5 MPa. To mitigate loss of containment risks, injection rates should remain below 6796 m^3/d. Future extension of this work should include micro-fracture testing, capillary entry pressure modeling, and geochemical analysis to assess the effects of mineral trapping. Expanding this conceptual workflow into a full-scale 3D model to capture the complexities of stress distribution and evaluating the practicality of using low injection rates will be essential for refining these findings and optimizing safe CO_2 storage strategies.

CRediT authorship contribution statement

Adrian Ross: Conceptualization, Methodology, Software, Investigation, Data Curation, Writing - original draft preparation. **David Alexander:** Supervision, writing - review & editing.

Declaration of Competing Interest

The authors declare that they have no known competing financial interests or personal relationships that could have appeared to influence the work reported in this paper.

Acknowledgments

We would like to thank CMG for the use of their software.

Data availability statement

All data included in this study are available upon reasonable request by contact with the corresponding author.

References

[1] D. Boodlal, Grant funded carbon management project with MEEI, 2018.
[2] V. Vilarrasa, S. Olivella, J. Carrera, Geomechanical stability of the caprock during CO_2 sequestration in deep saline aquifers, Energy Procedia 4 (2011) 5306–5313.
[3] J. Rutqvist, C.F. Tsang, A study of caprock hydromechanical changes associated with CO_2-injection into a brine formation, Env. Geol. 42 (2002) 296–305.
[4] G.W. Kim, T.H. Kim, J. Lee, et al., Coupled geomechanical-flow assessment of CO_2 leakage through heterogeneous caprock during CCS, Adv. Civ. Eng. 1 (2018) 1474320.
[5] J. Rutqvist, D.W. Vasco, L. Myer, Coupled reservoir-geomechanical analysis of CO_2 injection and ground deformations at In Salah, Algeria, Int. J. Greenh. Gas Control 4 (2) (2010) 225–230.
[6] A. Gillioz, F. Verga, C. Deangeli, Critical parameters for caprock tensile failure induced by CO_2 injection into aquifers, in: SPE Europe Energy Conference and Exhibition, Turin, Italy (2024) SPE-220097-MS.
[7] A. Alvarez, D. Mercado, V. Salazar, Modeling caprock failure during injection in a CO_2 capture and storage project using a compositional/geochemical/geomechanical coupled numerical simulation, in: SPE Latin American and Caribbean Petroleum Engineering Conference, Port of Spain, Trinidad and Tobago (2023) SPE-213135-MS.
[8] K. Narayanan, A. Herris, J. O'Sullivan, et al., Angostura phase 3-rejuvenating complex turbidite fields in offshore Trinidad through a successful subsea tieback project, in: SPE Latin American and Caribbean Petroleum Engineering Conference, Virtual (2020) SPE-199019-MS.
[9] A. Busch, A. Amann, P. Bertier, et al., The significance of caprock sealing integrity for CO_2 storage, in: SPE International Conference on CO_2 Capture, Storage, and Utilization, New Orleans, Louisiana, USA (2010) SPE-139588-MS.
[10] CMG Ltd, Gem user guide—compositional & unconventionalreservoir simulation, version 2022, Computer Modeling Group Ltd, Calgary, 2022. (accessed 8 Sep 2024).
[11] Z.W. Dai, L.Q. Wang, K.Q. Zhang, et al., Implementation of the Barton–Bandis nonlinear strength criterion into Mohr–Coulomb sliding failure model, Adv. Mater. Sci. Eng. 1 (2022) 1590884.
[12] H. Belyadi, E. Fathi, F. Belyadi, Rock mechanical properties and in situ stresses, in: Hydraulic Fracturing in Unconventional Reservoirs, 2019, Elsevier, 215–231.
[13] J.F. Labuz, A. Zang, Mohr–Coulomb failure criterion, Rock Mech. Rock Eng. 45 (6) (2012) 975–979.
[14] H. Jiang, Y.L. Xie, A note on the Mohr–Coulomb and Drucker–Prager strength criteria, Mech. Res. Commun. 38 (4) (2011) 309–314.
[15] S. Archer, V. Rasouli, A log based analysis to estimate mechanical properties and in-situ stresses in a shale gas well in North Perth Basin, WIT Trans. Eng. Sci. 81 (2012) 163–174.
[16] J.P. Castagna, M.L. Batzle, T.K. Kan, et al., Rock physics—the link between rock properties and AVO response, in: Offset-Dependent Reflectivity-Theory and Practice of AVO Analysis, Society of Exploration Geophysicists, Houston, 1993, pp. 135–171.
[17] K. Ramcharitar, R. Hosein, Rock mechanical properties of shallow unconsolidated sandstone formations, in: SPE Trinidad and Tobago Section Energy Resources Conference, Port of Spain, Trinidad and Tobago (2016) SPE–180803-MS.

[18] S.K. Zhang, S.D. Yin, Y.G. Yuan, Estimation of fracture stiffness, in situ stresses, and elastic parameters of naturally fractured geothermal reservoirs, Int. J. Geomech. 15 (1) (2015) 04014033.
[19] X.P. He, M. Sinan, H. Kwak, et al., A corrected cubic law for single-phase laminar flow through rough-walled fractures, Adv. Water Resour. 154 (2021) 103984.
[20] J.F.W. Gale, S.E. Laubach, J.E. Olson, et al., Natural fractures in shale: A review and new observations, AAPG Bull. 98 (11) (2014) 2165–2216.
[21] S.M. Ghaderi, D.W. Keith, Y. Leonenko, Feasibility of injecting large volumes of CO_2 into aquifers, Energy Procedia 1 (1) (2009) 3113–3120.
[22] C.M. Oldenburg, P.D. Jordan, J.P. Nicot, et al., Leakage risk assessment of the In Salah CO_2 storage project: Applying the certification framework in a dynamic context, Energy Procedia 4 (2011) 4154–4161.
[23] Carbon Capture and Sequestration Technologies MIT, In Salah fact sheet: Carbon dioxide capture storage project (2016). ⟨https://sequestration.mit.edu/tools/projects/in_salah.html⟩ (accessed 11 Oct 2024).
[24] P.S. Ringrose, A.S. Mathieson, I.W. Wright, et al., The In Salah CO_2 storage project: Lessons learned and knowledge transfer, Energy Procedia 37 (2013) 6226–6236.
[25] A. Mathieson, I. Wright, D. Roberts, et al., Satellite imaging to monitor CO_2 movement at Krechba, Algeria, Energy Procedia 1 (1) (2009) 2201–2209.
[26] G.A. Williams, R.A. Chadwick, Influence of reservoir-scale heterogeneities on the growth, evolution and migration of a CO_2 plume at the Sleipner Field, Norwegian North Sea, Int. J. Greenh. Gas Control 106 (2021) 103260.
[27] A. Baklid, R. Korbol, G. Owren, Sleipner vest CO_2 disposal, CO_2 injection into a shallow underground aquifer, in: SPE Annual Technical Conference and Exhibition, Denver, Colorado (1996) SPE-36600-MS.
[28] T.A. Torp, J. Gale, Demonstrating storage of CO_2 in geological reservoirs: The sleipner and SACS projects, Energy 29 (9–10) (2004) 1361–1369.
[29] V. Vandeweijer, C. Hofstee, van W. Pelt, et al., CO_2 injection at K12-B, the final story, in: Proceedings of the 15th Greenhouse Gas Control Technologies Conference (2021).
[30] V. Vandeweijer, C. Hofstee, H. Graven, 13 years of safe CO_2 injection at K12-B, in: Fifth CO_2 Geological Storage Workshop, Utrecht, Netherlands (2018).
[31] P. Audigane, J. Lions, I. Gaus, et al., Geochemical modeling of CO_2 injection into a methane gas reservoir at the K12-B field, North Sea, in: M. Grobe, J.C. Pashin, R. L. Dodge (Eds.), Carbon Dioxide Sequestration in Geological Media—State of the Science, American Association of Petroleum Geologists, 2009.
[32] C.D. Chang, M.D. Zoback, A. Khaksar, Empirical relations between rock strength and physical properties in sedimentary rocks, J. Pet. Sci. Eng. 51 (3–4) (2006) 223–237.
[33] G.J. Gonzalez Martinez de Miguel, A hydromechanically-based risk framework for CO_2 storage coupled to underground coal gasification, PhD Thesis, Newcastle University, Newcastle upon Tyne, UK (2014).
[34] S.E. Saberhosseini, R. Keshavarzi, K. Ahangari, A new geomechanical approach to investigate the role of in-situ stresses and pore pressure on hydraulic fracture pressure profile in vertical and horizontal oil wells, Geomech. Eng. 7 (3) (2014) 233–246.
[35] M. Ziaie, M. Fazaelizadeh, A.A. Tanha, et al., Estimation of the horizontal in-situ stress magnitude and azimuth using previous drilling data, Petroleum 9 (3) (2023) 352–363.
[36] C.M. Sayers, The effect of anisotropy on the Young's moduli and Poisson's ratios of shales, Geophys. Prospect. 61 (2) (2013) 416–426.

Adrian Ross is a multi-discipline energy professional with over 16 years of experience across the energy sector, including petrochemical plants, production platforms, FPSOs, and infill drilling campaigns, spanning construction, commissioning, and maintenance. His expertise covers electrical and instrumentation systems, production operations, and reservoir optimization. Mr. Ross holds a Master of Philosophy in Energy Studies, which focused on geomechanical risks associated with CO_2 storage in depleted gas reservoirs, as well as a Master of Engineering in Petroleum Engineering with a specialization in renewable energy, and a technical diploma in Electrical and Electronics Engineering. His current research interests include geothermal energy systems, CO_2 storage and caprock integrity under geomechanical constraints, and the application of artificial intelligence for developing surrogate models to predict CO_2 storage performance.

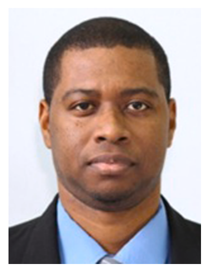

Prof. David Alexander is the current Programme Leader of the Energy Systems Engineering Unit at the University of Trinidad and Tobago (UTT) since 2014. He is also a consultant in the areas of Energy and the Environment, having worked on several projects in the region. He holds a Bachelor of Science (B.Sc.) in Chemistry/Analytical Chemistry and a Master of Science (M.Sc.) in Petroleum Engineering from the University of the West Indies, an M.Sc. in Information and Communication Technology with specialization in Software Engineering from UTT, and a Doctor of Philosophy (Ph.D.) in the field of Petroleum Engineering from UTT in collaboration with the University of Texas at Austin. Prof. Alexander currently leads research in the areas of Enhanced Oil Recovery, Carbon Capture and Storage, and Waste Management, among other areas. He has over 50 publications, with over 30 published in international journals.